Bright Betatronlike X Rays from Radiation Pressure Acceleration of a Mass-Limited Foil Target

Tong-Pu Yu (余同普),[1,2,3,*] Alexander Pukhov,[3,†] Zheng-Ming Sheng (盛政明),[4] Feng Liu (刘峰),[5,4] and Gennady Shvets[6]

[1]*Department of Physics, National University of Defense Technology, Changsha 410073, China*
[2]*State Key Laboratory of High Performance Computing, National University of Defense Technology, Changsha 410073, China*
[3]*Institut für Theoretische Physik I, Heinrich-Heine-Universität Düsseldorf, 40225 Düsseldorf, Germany*
[4]*Key Laboratory for Laser Plasmas (MoE) and Department of Physics, Shanghai Jiao Tong University, Shanghai 200240, China*
[5]*Institut für Laser-und Plasmaphysik, Heinrich-Heine-Universität Düsseldorf, 40225 Düsseldorf, Germany*
[6]*Department of Physics, The University of Texas at Austin, Austin, Texas 78712, USA*

(Received 3 May 2012; published 23 January 2013)

By using multidimensional particle-in-cell simulations, we study the electromagnetic emission from radiation pressure acceleration of ultrathin mass-limited foils. When a circularly polarized laser pulse irradiates the foil, the laser radiation pressure pushes the foil forward as a whole. The outer wings of the pulse continue to propagate and act as a natural undulator. Electrons move together with ions longitudinally but oscillate around the latter transversely, forming a self-organized helical electron bunch. When the electron oscillation frequency coincides with the laser frequency as witnessed by the electron, betatronlike resonance occurs. The emitted x rays by the resonant electrons have high brightness, short durations, and broad band ranges which may have diverse applications.

DOI: 10.1103/PhysRevLett.110.045001 PACS numbers: 52.38.Kd, 41.60.Ap, 52.38.Ph, 52.59.Px

With the rapid development of large scale instruments like synchrotrons, research of x-ray radiation has made significant progress in the last decades. The brightness of the radiation has continuously increased and the duration has greatly decreased. This makes it possible to probe and image electric, atomic, and molecular fundamental events at nanosecond and even femtosecond time scales. Despite the demand in practice, there are only a few dedicated synchrotron facilities worldwide, partially due to the size and cost of the conventional accelerators [1]. Previous studies have shown that laser-produced plasma is also a promising medium for secondary radiation generation [2,3]. In the laser-driven wakefield accelerator (LWFA) for electrons [4], free electrons of the plasma can be trapped and accelerated in the laser propagation direction by the wakefield. Meanwhile, these electrons are subjected to a radial restoring force of space-charge separation field and simultaneously oscillate in the transverse direction, which is referred to as betatron oscillation [2]. The relativistic and oscillatory motion of electrons is able to emit collimated synchrotron radiation with spectra peaking between 1 and 10 keV [5]. Recent research also showed that the oscillation amplitude could be enhanced when electrons interact with the rear of laser pulses. The photon energies were significantly increased and bright femtosecond duration γ rays were thus observed in experiments [6].

Previous research of laser-produced x rays has focused on laser low-density plasma interaction in LWFA. Recently, radiation pressure acceleration (RPA [7]) of thin solid foils has been extensively studied due to its high energy conversion efficiency, which might provide us with an excellent opportunity to produce ultraintense, ultrashort, ultrabright x rays and even γ rays. In the RPA regime, the laser radiation pressure as high as a few Gbar is able to accelerate the nm foil forward as a whole, which intrinsically holds the promise of producing monoenergetic ion beams with densities well above the critical density [8]. In the field of a circularly polarized laser pulse, electrons may be dragged out from the foil and move in circular orbits, resulting in strong transverse charge separation fields [9]. In the longitudinal direction, electrons can be significantly accelerated together with the protons by the laser pressure. Thus, a betatronlike oscillation is expected. For electrons undergoing betatron oscillations, the average total radiation power is proportional to $(\gamma_e n_p r_0)^2$, where γ_e is the relativistic factor of the electron, n_p is the ion density, and r_0 is the radial excursion of the electron [2]. Considering the high ion densities in RPA, we may obtain high power synchrotron radiation with high photon energies provided the electron oscillation amplitude is large enough.

In this Letter, we report the first numerical observation of bright resonant hard x-ray emission from radiation pressure acceleration of ultrathin mass-limited foils. With the help of multidimensional particle-in-cell (PIC) simulations with the radiation reaction (RR) effect incorporated, it is shown that the central part of a circularly polarized laser pulse exerts radiation pressure on the foil and pushes the foil forward as a whole. The outer wings of the pulse continue to propagate, envelop the foil, and transversely confine the electrons. Under the combined action of the laser radiation pressure and transverse laser

field, electrons move longitudinally together with ions and transversely oscillate around the latter. A self-organized helical electron bunch is thus formed and ultrabright ultrashort x rays are emitted. The underlying physics is discovered, which can be attributed to the betatronlike resonance introduced energy coupling between the laser and electrons. The emitted x rays have promising features, such as compact sizes, high brightness, short durations, and broad band ranges.

In order to study the electromagnetic emission in the RPA regime, we first have to modify the PIC code. The short wavelength radiation is completely out of the conventional PIC scope and must be included in a model way [2,3]. The radiation spectrum is calculated assuming that an angular distribution is peaked in the direction of the electron momentum and can be approximated with the δ function and the frequency spectrum $S(\omega/\omega_c)$, where $S(x) = x\int_x^\infty K_{5/3}(\xi)d\xi$ and $\omega_c = (3/4\pi)\gamma^2|\triangle P_\perp|/dt$ is the critical frequency, $\gamma = (1 + p_\parallel^2 + p_\perp^2)^{1/2}$ is the relativistic factor, and $\triangle P_\perp$ is the variation of the transverse electron momentum force during the time step dt [10]. In the code VLPL [11], a recoil on the electron exerted by the emitted radiation is included into the equations of the electron motion by [10]

$$f_{\rm rad} = \frac{4}{9}\alpha\frac{3\gamma^2}{4\pi}\frac{E_{\rm ph}({\rm eV})}{5.11\times10^5}\left(\frac{dp_\perp}{dt}\right)^2, \qquad (1)$$

where $\alpha = e^2/\hbar c = 1/137$ is the fine-structure constant, $E_{\rm ph} = \hbar\omega_0$ is the laser photon energy, $\hbar$ is the Planck constant, $\omega_0 = 2\pi c/\lambda_0$ is the laser frequency, λ_0 is the laser wavelength, and c is the speed of light in vacuum. Thus, during the time step dt, the radiated photon number is characterized by $n_{\rm ph} = (4/9)\alpha dp_\perp$. The recoil contribution is added in the code after the normal push by the Lorentz force. By multiplying Eq. (1) by the particle velocity $\boldsymbol{v}$ and retaining the leading term, we recover the textbook [12,13] equation of motion with the radiation reaction. This gives the same power of the radiation emission. The approach can be extended to the quantum regime easily when the photon energy becomes comparable with the electron energy. The model and approach have been verified by several experiments and independent simulations [1,5,6,14]. In the following, we make use of the modified code to explore the electron and ion dynamics as well as synchrotron radiation in the RPA regime.

We first carry out 3D simulations to show a general picture of the laser mass-limited foil interaction. The simulation box is $x\times y\times z = 16\lambda_0\times15\lambda_0\times15\lambda_0$, sampled by $3200\times300\times300$ cells with 16 particles in each cell. The time step is $\Delta t = 0.0045T_0$, where $T_0 = 3.3$ fs is the laser cycle. A moving window is employed for computational efficiency. A circularly polarized super-Gaussian laser pulse with a transverse profile $a = a_0\exp(-r^8/\sigma_L^8)$ is incident from the left side onto a thin flat hydrogen foil, where $a_0 = 100$ is the dimensionless laser field amplitude and $\sigma_L = 4\sqrt{2}\lambda_0$ is the focal radius. The laser pulse has a trapezoidal profile in time (linear up-ramp $= 1T_0$, plateau $= 10T_0$, linear down-ramp $= 1T_0$). The foil is located at $x = 5.0$–$5.1\lambda_0$ with a transverse size of $8\lambda_0\times8\lambda_0$ which is comparable to the laser focal spot (namely "mass-limited" foil, MLF). The plasma density is $n_e = 320n_c$ where $n_c = m_e\omega_0^2/4\pi e^2$ is the plasma critical density.

Figure 1(a) shows the typical evolutions of electron and proton isocontour surfaces. During the laser-MLF interaction, we can see a very clear rotation structure of electrons around the center proton bunch. The structure is very stable and can be kept for a long time, e.g., $t\sim\tau_L$. It is the first time to find such a compact helical electron bunch with densities well above n_c in laser-plasma interaction. Interestingly, the radius of the helix structure becomes larger with time, which indicates the increase of the electron energies [2]. Figure 1(b) shows the distribution of proton densities in the x-y plane and electric fields E_y in the x-z plane at $t = 15T_0$. As we can see, the laser wing pulse overtakes the foil from the boundaries and envelops the foil, forming an inverted cone. The foil acceleration can be divided into several stages. At the very beginning, electrons instantly move in front of protons because of the faster response of electrons to the laser pulse. A space-charge separation field is thus formed which pulls the ions forward together with electrons. At this stage, the laser radiation pressure is balanced by the potential of the separation field and the foil velocity can be expressed as

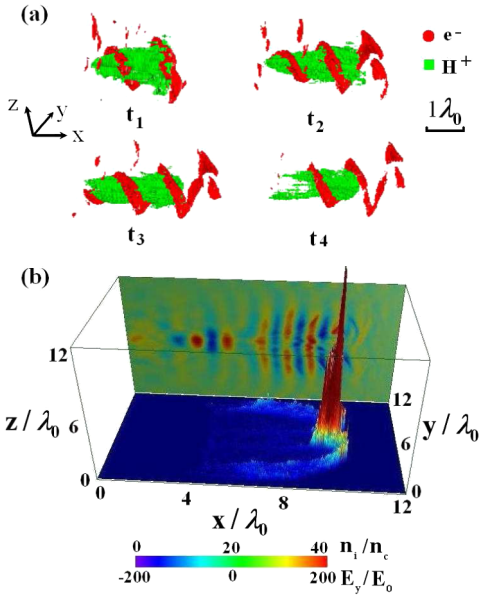

FIG. 1 (color online). (a) 3D evolutions of electrons and protons at $t_1 = 17.5T_0$, $t_2 = 20T_0$, $t_3 = 22.5T_0$, and $t_4 = 25T_0$. For smooth visualization, we show both with densities above $8n_c$. (b) Projections of proton density distributions in the x-y plane and transverse electrical fields E_y in the x-z plane. Here, the field is normalized to $m_e c\omega_0/e = 3.2\times10^{12}$ V/m.

$$\beta_{i,e}(t) = 1 - [\zeta(t) + \xi(t)]^{1/3} - [\zeta(t) - \xi(t)]^{1/3}, \quad (2)$$

where $\zeta(t) = 1/[1 + h(t)^2]$, $\xi(t) = h(t)/[1 + h(t)^2]^{3/2}$, and $h(t) = 6It/m_i n_i Lc + 2$ with I, m_i and n_i being the laser intensity, the ion mass and density, respectively [15]. Gradually, the outer wings of the pulse overpass the foil boundaries, envelop the whole foil, and compress it so that its transverse size becomes much smaller than the laser focal spot. In the transverse electric field of the surpassing pulse, $\boldsymbol{E}_\perp = \boldsymbol{E}_y + \boldsymbol{E}_z$, electrons in the originally compressed bunch are continually pulled out. In each laser cycle, the electron bunch shows a longitudinal interval of about $1\lambda_0$ as seen in Fig. 1(a). In sharp contrast to the slice structures in the case with linearly polarized lasers [16], such a tight self-organized bunch leads to the generation of circulating electrons. Meanwhile, the protons keep an intact acceleration structure with a pronounced density peak as shown in Fig. 1(b). At this stage, electrons manifest a complicated acceleration picture. On the one hand, they oscillate in the surpassing laser transverse field with the same frequency of the laser pulse; on the other hand, the displacement between electrons and protons results in a strong radial restoring force, through which electrons execute a betatronlike oscillation. As in LWFA, the force can also act as an effective wiggler or undulator for synchrotron radiation.

In order to get insight into dynamics of the laser-MLF interaction, we perform 2D simulations with a longer laser duration ($\tau_L = 22T_0$) and larger focal spot ($\sigma_L = 8\sqrt{2}\lambda_0$) but faster computation. The foil size is $0.1\lambda_0 \times 16\lambda_0$ and the simulation box is $x \times y = 50\lambda_0 \times 30\lambda_0$ with 800 particles in each cell. The super-Gaussian laser pulse has a peak intensity $a_0 = 100$ and all the other parameters are the same as in the 3D case. Figure 2 shows the simulation results. The slice structure with a duration of ~200 as and an interval of $\sim 1\lambda_0$ in Fig. 2(a) is actually x-y projection of the rotation rings as seen in three dimensions. The overtaking laser pulse from the boundaries of the MLF is also clear in Fig. 2(c), which envelops the foil and compresses it into a small "conelike" bunch. The attosecond electron slices are continually pulled out by the intense laser field from the compressed bunch which can be regarded as an electron injection source. Figure 2(b) shows the proton density distribution and the energy spectrum at $t = 80T_0$. As expected, a compact monoenergetic proton bunch with a peak energy of ~1.5 GeV and an energy spread of ~8% is obtained, which is one of the best results for proton acceleration in the RPA regime [7,8]. Figure 2(d) presents the electron energy distribution in space at $t = 120T_0$. The stable structure of the slice can be kept for a very long time, e.g., 250 fs after the laser-MLF interaction. It is ten times longer than in the linearly polarized laser case where electron heating exists and diffuses the electron bunches soon [16]. Figure 2(e) shows the phase space distribution of electrons at $t = 120T_0$. Many electrons oscillate with $p_y/m_e c \sim 400 > a_0$, which implies interesting physics

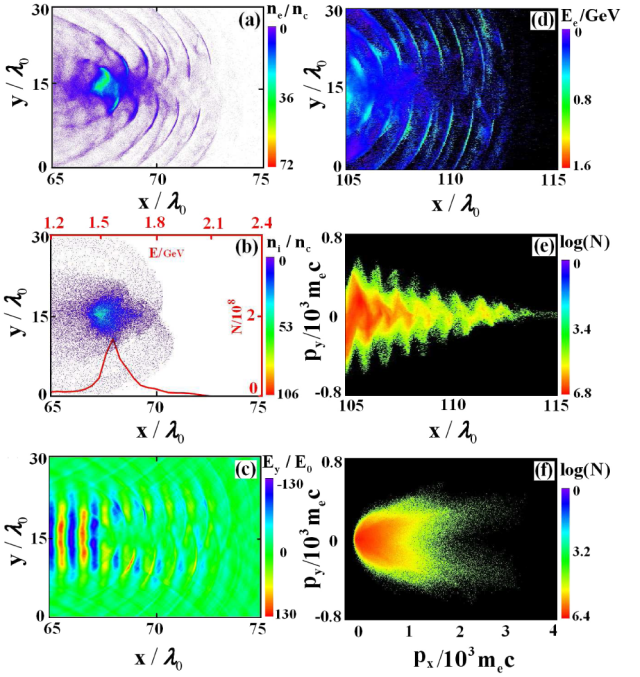

FIG. 2 (color online). 2D simulations of the laser-MLF interaction. (a), (b), (c) The distributions of the electron density, the proton density, and the laser field E_y at $t = 80T_0$. The red curve in (b) shows the proton energy spectrum. (d), (e), (f) The distributions of the electron energy, phase space, and divergency p_y: p_x at $t = 120T_0$.

inside the accelerated target. In our case, we finally obtain electrons with an unexpectedly high energy (~750 MeV) and density ($\sim 5n_c$). This is beyond the predictions of the 1D "light-sail" model [7], from which we can obtain only tens MeV electron kinetic energies. Meanwhile, the energy is also much higher than the electron ponderomotive energy $(\sqrt{1 + a_0^2/2} - 1)m_e c^2 = 36$ MeV.

The circulating electrons and their high energies play a critical role in the final synchrotron radiation. We interpret the high electron energy by the schematic diagram as shown in Fig. 3(a). Here, the laser electric field can be written as $\boldsymbol{E} = \boldsymbol{E}_0 e^{-i(\omega_0 t - kx)}$ with $E_0 = m_e c\omega_0 a_0/e$. The laser frequency as witnessed by an electron at a specific location $x_t = v_\parallel t$ can be written by $\Omega = \omega_0 - kv_\parallel = \omega_0(1 - \beta_\parallel)$, where $\beta_\parallel$ can be approximated by $\beta_{i,e}$ initially. Due to the radial restoring force, the electron oscillates around the proton bunch at a frequency comparable to $\omega_\beta = (4\pi e^2 n_i/2\gamma_e m_e)^{1/2}$. It is a high frequency oscillation and the charge separation field that the protons feel is averaged so that the protons can form a compact bunch and keep intact during the acceleration. When the oscillation frequency of the electron gets close to the laser frequency seen by the electron, i.e., $\omega_\beta \sim \Omega$, betatronlike resonance takes place, enabling an efficient energy coupling between the laser and electrons. Thus, the resonance condition can be written as

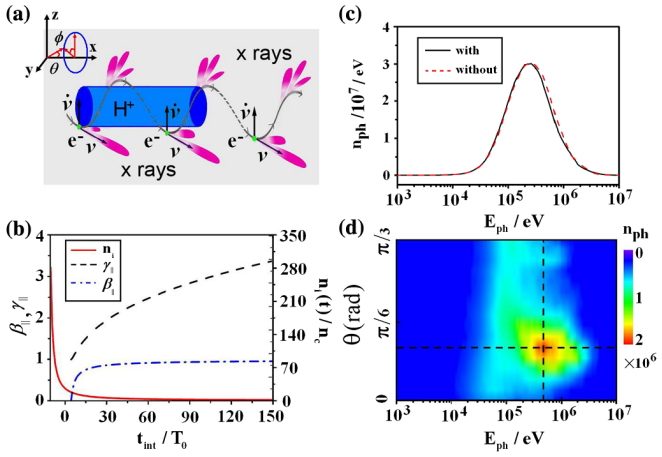

FIG. 3 (color online). (a) Schematic of x-ray emission in the laser-MLF interaction. (b) Analytical evolutions of $\beta_{\parallel}$, $\gamma_{\parallel}$, and $n_i(t)$. Here, $t_{\rm int} = t - 5$ refers to the interaction time. (c) Radiation spectra with and without considering the RR effect. (d) Angular dependence of the radiation on the photon energies. Here, θ is the angle between the emission and the laser propagation direction.

$$1 - \beta_{\parallel} - \sqrt{\frac{n_i/n_c}{2\gamma_e}} \sim 0. \tag{3}$$

Considering $\beta_{\parallel} = p_{\parallel}/(1 + p_{\parallel}^2 + p_{\perp}^2)^{1/2}$ and noting that $\beta_{\parallel} = v_{\parallel}/c = (1 - 1/\gamma_{\parallel}^2)^{1/2}$, we thus obtain $p_{\parallel}^2 = (\gamma_{\parallel}^2 - 1)(1 + \mu^2 a_0^2)$, where we assume $p_{\perp} = \mu a_0$ with the parameter μ characterizing the occurrence of the resonance. For the case $\mu \sim 1$, $p_{\perp} \sim a_0$, and $p_{\parallel} \sim (\gamma_{\parallel}^2 - 1)^{1/2} a_0$ indicate that no resonance takes place. When $\mu > 1$, we have $p_{\perp} \gg a_0$ and $p_{\parallel} \sim (\gamma_{\parallel}^2 - 1)^{1/2}\mu a_0$ as a result of betatronlike resonance. In the RPA regime under consideration with $a_0 = 100 \gg 1$, we may estimate the energy of a resonant electron by $\gamma_e = [1 + \mu^2 a_0^2(\gamma_{\parallel}^2 + 1)]^{1/2} \approx (\gamma_{\parallel}^2 + 1)^{1/2}\mu a_0$. Assuming electrons initially to be accelerated at a longitudinal velocity $\beta_{i,e}$ and $p_{\perp} \sim a_0$, we can rewrite the resonance condition by the local ion density

$$\frac{n_i(t)}{n_c} \sim 2(1 - \beta_{\parallel})^2 a_0 \sqrt{\frac{2 - \beta_{\parallel}^2}{1 - \beta_{\parallel}^2}}, \tag{4}$$

where $n_i(t)$ presents the critical value of the ion density for the resonance as marked by the red curve in Fig. 3(b). During the laser-MLF interaction, the electron longitudinal velocity β_e increases but the ion density n_i decreases. When the ion density reduces to the critical value by Eq. (4), betatronlike resonance takes place and high energy electrons are generated which accounts for the increasing oscillation amplitude of the helical electron bunch as seen in Fig. 1(a). Obviously, the high electron energies, the large oscillation amplitudes, as well as the high ion densities are desirable for electrons to emit intense synchrotron radiation. The estimation and analysis above agree well with the numerical observations as shown in Figs. 2(d)–2(f). In the simulations, we get the maximum $p_x/m_e c = 2000$ and $p_y(p_z)/m_e c = 380 \approx 4a_0$ at $t = 120T_0$, validating that the transverse motion of the electrons is essentially oscillations driven resonantly by the laser field. Taking $\mu = 4$ and $\gamma_{\parallel} = \gamma_H = 3.3$ [$E_H \approx 2.1$ GeV, see Fig. 3(b)], we can estimate the energy of resonant electrons $\gamma_e = 1380$. It is in excellent agreement with the simulation results as shown in Fig. 2(d). Additionally, we also find that the required ion density for the resonance is only tens n_c at $t \sim 25T_0$. This is easily satisfied in the simulations so that betatronlike resonance can thus take place.

We finally discuss the electromagnetic emission in the laser-MLF interaction. The emission is characterized by the radiated photon frequency and number recorded in every time step. For simplicity, we take into account only radiation by electrons with energies above 50 eV. Figure 3(c) presents the typical radiation spectra. The photon energy is as high as a few MeV which is much larger than in LWFA [5]. This can be attributed to the betatronlike resonance of electrons and large ion densities during the interaction. As we can see, the radiation spectrum shows a broad frequency band covering the total range from soft x rays to γ rays. The corresponding photon energy from 1 keV to 10 MeV is centered at about 300 keV, indicating that the radiation is essentially hard x rays. The fundamental radiation wavelength agrees well with the estimation for small-amplitude near-axis betatron oscillations by $\lambda_{\rm rad} = [1/(\gamma_e\sqrt{2\gamma_e})]\sqrt{n_c/n_e}\lambda_0$. This further demonstrates the betatronlike x-ray emission in our case. In order to show the role of the RR effect in x-ray emission, we also show the radiation spectrum in the case without considering the RR effect in Fig. 3(c). Obviously, both spectra are almost the same. This indicates that the RR effect has a low influence on the radiation at the current laser intensity. However, when we increase the laser intensity, e.g., $a = 200$, the difference is significant so that the RR effect must be taken into account.

Figure 3(d) shows the angular dependence of the radiation on the photon energies. Here, θ is the angle between the emission and the laser propagation direction. As in LWFA, the radiation is confined within a small cone, e.g., $1/\gamma_e \sim 0.8$ mrad, at $t = 130T_0$. Obviously, the emitted x rays are dominantly in the forward direction at a small angle with a center frequency around 300 keV. At the observation angle $\theta \sim \pi/9$, the x rays have high brightness with more than 10^{10} photons. Meanwhile, they have ultrashort durations, e.g., $t \sim 10$ fs as shown in Fig. 1(a) and are elliptically polarized. Additionally, we may obtain bright soft x rays and γ rays by varying the foil and laser parameters. Typically, we can reduce the foil density n_e and laser intensities to obtain bright XUV and soft x rays which might be approachable in current laboratories. This is the first finding of such short brilliant conelike

x rays by electrons at betatronlike resonance in the RPA regime. The emitted x rays and γ rays might have diverse applications in imaging, isotope production, following the evolution of chemical processes, and initiating photonuclear reactions [17].

In conclusion, we report the first numerical observation of bright hard x-ray emission by resonant electrons from radiation pressure acceleration of ultrathin MLFs. By using 3D and 2D PIC simulations, it is shown that electrons oscillate in the laser field and are simultaneously subjected to a radial restoring force of ion beams. Bright short-duration x rays with a broad frequency band range are thus emitted in a cone. The underlying physics is discovered, which can be attributed to the betatronlike resonance introduced energy coupling between the laser and electrons. The emitted hard x rays have promising features and might serve as a new compact short-wavelength light source in the future.

This work is financially supported by NSFC (Grants No. 11205243, No. 91230205, No. 11175253, and No. 11175255) and NSAF (Grant No. 10976031). A. P. and F. L. acknowledge the support of DFG program TR18. Z. M. S. acknowledges the support by NSFC (Grants No. 11121504 and No. 10935002). G. S. acknowledges the support of the U.S. DOE Grant No. DE-FG02-04ER41321. The simulations were performed on Tianhe-1 at National Super-Computer Center in Changsha (NSCC-CS).

*tongpu@nudt.edu.cn
†pukhov@tp1.uni-duesseldorf.de

[1] S. Kneip *et al.*, Nat. Phys. **6**, 980 (2010).
[2] A. Pukhov, Z.-M. Sheng, and J. Meyer-ter-Vehn, Phys. Plasmas **6**, 2847 (1999); I. Kostyukov, S. Kiselev, and A. Pukhov, Phys. Plasmas **10**, 4818 (2003); S. Kiselev, A. Pukhov, and I. Kostyukov, Phys. Rev. Lett. **93**, 135004 (2004).
[3] E. Esarey, B. A. Shadwick, P. Catravas, and W. P. Leemans, Phys. Rev. E **65**, 056505 (2002).
[4] T. Tajima and J. M. Dawson, Phys. Rev. Lett. **43**, 267 (1979); A. Pukhov and J. Meyer-ter-Vehn, Appl. Phys. B **74**, 355 (2002).
[5] A. Rousse *et al.*, Phys. Rev. Lett. **93**, 135005 (2004); S. Corde, K. Phuoc, R. Fitour, J. Faure, A. Tafzi, J. Goddet, V. Malka, and A. Rousse, Phys. Rev. Lett. **107**, 255003 (2011); M. Schnell *et al.*, Phys. Rev. Lett. **108**, 075001 (2012).
[6] S. Cipiccia *et al.*, Nat. Phys. **7**, 867 (2011).
[7] F. Pegoraro and S. V. Bulanov, Phys. Rev. Lett. **99**, 065002 (2007); A. P. L. Robinson, M. Zepf, S. Kar, R. G. Evans, and C. Bellei, New J. Phys. **10**, 013021 (2008); A. Macchi, S. Veghini, and F. Pegoraro, Phys. Rev. Lett. **103**, 085003 (2009); T. P. Yu, M. Chen, and A. Pukhov, Laser Part. Beams **27**, 611 (2009); H. B. Zhuo, Z. Chen, W. Yu, Z. Sheng, M. Yu, Z. Jin, and R. Kodama, Phys. Rev. Lett. **105**, 065003 (2010).
[8] X. Q. Yan, C. Lin, Z. Sheng, Z. Guo, B. Liu, Y. Lu, J. Fang, and J. Chen, Phys. Rev. Lett. **100**, 135003 (2008); M. Chen, A. Pukhov, T. P. Yu, and Z. M. Sheng, Phys. Rev. Lett. **103**, 024801 (2009); B. Qiao, M. Zepf, M. Borghesi, and M. Geissler, Phys. Rev. Lett. **102**, 145002 (2009); A. Henig *et al.*, Phys. Rev. Lett. **103**, 245003 (2009); T. P. Yu, A. Pukhov, G. Shvets, and M. Chen, Phys. Rev. Lett. **105**, 065002 (2010); S. V. Bulanov, E. Yu. Echkina, T. Zh. Esirkepov, I. N. Inovenkov, M. Kando, F. Pegoraro, and G. Korn, Phys. Rev. Lett. **104**, 135003 (2010).
[9] F. He, Y. Wei, L. Peixiang, X. Han, S. Baifei, L. Ruxin, and X. Zhizhan, Plasma Sci. Technol. **7**, 2968 (2005); Y. I. Salamin, Phys. Lett. A **283**, 37 (2001); S. G. Rykovanov, J. Schreiber, J. Meyer-ter-Vehn, C. Bellei, A. Henig, H. C. Wu, and M. Geissler, New J. Phys. **10**, 113005 (2008).
[10] M. Chen, A. Pukhov, T.-P. Yu, and Z.-M. Sheng, Plasma Phys. Controlled Fusion **53**, 014004 (2011).
[11] A. Pukhov, J. Plasma Phys. **61**, 425 (1999).
[12] L. D. Landau and E. M. Lifshitz, *The Classical Theory of Fields* (Pergamon, London, 1979), 4th ed.
[13] F. Rohrlich, Phys. Lett. A **303**, 307 (2002).
[14] C. P. Ridgers, C. Brady, R. Duclous, J. Kirk, K. Bennett, T. Arber, A. Robinson, and A. Bell, Phys. Rev. Lett. **108**, 165006 (2012).
[15] T. P. Yu, A. Pukhov, G. Shvets, M. Chen, T. H. Ratliff, S. A. Yi, and V. Khudik, Phys. Plasmas **18**, 043110 (2011).
[16] N. Naumova, I. Sokolov, J. Nees, A. Maksimchuk, V. Yanovsky, and G. Mourou, Phys. Rev. Lett. **93**, 195003 (2004); Y.-Y. Ma, Z.-M. Sheng, Y.-T. Li, W.-W. Chang, X.-H. Yuan, M. Chen, H.-C. Wu, J. Zheng, and J. Zhang, Phys. Plasmas **13**, 110702 (2006); T. V. Liseykina, S. Pirner, and D. Bauer, Phys. Rev. Lett. **104**, 095002 (2010).
[17] G. Shvets, Nat. Phys. **7**, 834 (2011).